
Individual predictions matter: Assessing the effect of data ordering in training fine-tuned CNNs for medical imaging

John R. Zech*
Department of Radiology
Columbia University Irving Medical Center
New York, NY
jrz2111@columbia.edu

Jessica Zosa Forde*, Michael L. Littman
Department of Computer Science
Brown University
Providence, RI
jessica_forde@brown.edu
mlittman@cs.brown.edu

Abstract

We reproduced the results of CheXNet with fixed hyperparameters and 50 different random seeds to identify 14 finding in chest radiographs (x-rays). Because CheXNet fine-tunes a pre-trained DenseNet, the random seed affects the ordering of the batches of training data but not the initialized model weights. We found substantial variability in predictions for the same radiograph across model runs (mean $\ln(P_{\max}/P_{\min})$ 2.45, coefficient of variation 0.543). This individual radiograph-level variability was not fully reflected in the variability of AUC on a large test set. Averaging predictions from 10 models reduced variability by nearly 70% (mean coefficient of variation from 0.543 to 0.169, t-test 15.96, p-value < 0.0001). We encourage researchers to be aware of the potential variability of CNNs and ensemble predictions from multiple models to minimize the effect this variability may have on the care of individual patients when these models are deployed clinically.

1 Introduction

While there is interest in using convolutional neural networks (CNNs) to identify findings in medical imaging [1–6], some researchers have questioned the reliability [7–11] and reproducibility [12–16] of deep learning methods. Often, researchers in medical imaging evaluate a single model’s predictions to measure performance [17, 18, 1, 19]. However, the loss surface of a CNN is non-convex, and differences in training such as random seed [16] and optimization method [20, 21] can affect the learned model weights and, consequently, the predictions of the model. Within the machine learning community, there are concerns that evaluation of a single trained model does not provide sufficient measurement of its variability [16, 11]. To mitigate this variability, some researchers in medical imaging have used cross-validation [22, 23], which varies the data used for both training and testing, but still uses a single model to make predictions during each cross-validation run. Others have used ensembling [24], combining predictions from 3 [25], 5 [26, 27], 10 [28–30], and 30 [2] different trained models to optimize classification performance. While ensembles have been proposed as a simple method for estimating the uncertainty of the predictions of a CNN [31, 32], such variability measurements, as seen in Wu et al. [26], are not common in medical imaging research.

If models generate different predictions when they are retrained, they may make inconsistent predictions for the same patient. The AUC of a single trained model will not give a direct indication of this inconsistency. AUC itself will likely vary between retrained models, which could complicate efforts to compare CNN performance to other models or human experts using statistical testing

*equal contribution

[33]. Researchers have attempted to quantify the uncertainty of predictions for individual patients by statistical estimation [34] and direct prediction [35]. Raghu et al. [35] proposed a machine learning method which identifies which retinal fundus photographs [28] would be likely to have human expert disagreement in diagnosing diabetic retinopathy; such a model could be used to identify high uncertainty cases likely to benefit from a second opinion. Dusenberry et al. [36] examined the variability of RNN-based mortality prediction using the medical records of ICU patients in MIMIC-III [3] and recommended the use of Bayesian RNNs [37] with stochastic embedding over ensembling as a way to estimate the variability of predictions in clinical time-series data.

In this study, we explicitly characterized the variability in individual predicted findings and overall AUC of a CNN that was trained multiple times to predict findings on chest radiographs. Like Dusenberry et al. [36], we found notable variability of predictions on individual patients with similar aggregate performance metrics. Because many real-world clinical decision support systems rely on single values of predicted probability rather than statistical distributions incorporating uncertainty, we focused our analysis on the use of ensembling for the purposes of robust prediction. We found that, in the case of chest radiographs, simple ensembling can reduce the variability of these probability estimates; ensembles of as few as ten models were found to reduce the variability of predictions by 70% (mean coefficient of variation from 0.543 to 0.169, t-test 15.96, p-value < 0.0001).

2 Methods

Using an open source implementation [38], we replicated the model described in Rajpurkar et al. [1] 50 times, varying the random seed with each fine-tuning [31]. Per Rajpurkar et al. [1], a DenseNet-121 [39] pre-trained on ImageNet [40] was fine-tuned to identify 14 findings in the NIH chest radiography dataset ($n=112,120$) [4]. The dataset was partitioned into 70% train, 10% tune, and 20% test data (train $n=78,468$, tune $n=11,219$, test $n=22,433$). These 50 models were fine-tuned using SGD with identical hyperparameters on the same train and tune datasets. Because the CNN was consistently initialized with parameters from a DenseNet-121 pre-trained to ImageNet, the only difference in the training procedure across model runs was the order in which data was batched and presented to the model during each epoch of fine-tuning. Each model’s performance was assessed on the full test partition ($n=22,433$). To replicate the test set used for labeling by radiologists [1], a smaller test partition ($n=792$) was created by randomly sampling 100 normal radiographs and 50 positive examples for each finding except for hernia ($n=42$ in the test set).

Table 1: Variability statistics for each finding on a radiograph in the test set across all 50 models. To measure the relative magnitude of predictions, we calculated the percentile rank of a prediction relative to all predictions for that finding in the test set and report the percentile rank range.

Metric	Symbol	Description (for each finding, radiograph pair)
Mean	μ	Average predicted probability
Stdev.	σ	Standard deviation of predicted probability
Coefficient of variation	σ/μ	Standard deviation divided by mean predicted probability
Log prob. ratio	$\ln(\frac{P_{\max}}{P_{\min}})$	Natural log of the highest predicted probability divided by the lowest predicted probability
Percentile (%ile) rank	$R(P)$	The percentile rank relative to all predictions for that finding among radiographs in the test set
%ile rank range	$R(P_{\max}) - R(P_{\min})$	The percentile rank of the highest probability predicted minus the percentile rank of the lowest probability predicted

We calculated various statistical measurements for each finding on each radiograph across our 50 models in the full test set ($n=22,433$). Table 1 describes each metric in detail. In addition to mean, standard deviation, and coefficient of variation, we calculated $\ln(\frac{P_{\max}}{P_{\min}})$, where P_{\max} is the greatest and P_{\min} the least probability predicted by the 50 trained models for a given finding on a given radiograph. This ratio provides a scaled measurement of the variability of the predicted probability of a finding on a radiograph. To contextualize predictions within the population of predictions for that finding, we calculated the percentile rank range of the predictions, $R(P_{\max}) - R(P_{\min})$, where $R(P)$ is the percentile rank of a prediction relative to all predictions for that finding in the test set.

To evaluate the effectiveness of ensembling in reducing variance, we averaged predictions over disjoint groups of 10 models to yield 5 separate averaged predictions for each finding for each radiograph ($n=5$ groups \times 10 models per group = 50 total models). We reported the standard deviation and coefficient of variation across these averaged groups. A paired t-test was used to compare coefficients of variation across the raw ($n=50$) and averaged ($n=5$) predictions.

We examined the variance in overall AUC for the 14 possible targets. For each of the 50 models, AUC was calculated on both the full and limited test sets using the pROC package in R [41, 42]. This calculation provided an empirical distribution of the test AUC relative to the order of samples in the training data. For both the full and limited test sets, we calculated the 95% confidence interval of this distribution by subtracting the second smallest AUC from the second largest of the 50 AUCs. For the limited test sets, the average width of the 95% confidence interval was also estimated using DeLong’s method [43] and bootstrapping [44]. DeLong expresses AUC in terms of the Mann-Whitney U statistic [45], a non-parametric test statistic that is approximately normally distributed for large sample size, and thus can be used to calculate confidence intervals.

3 Results

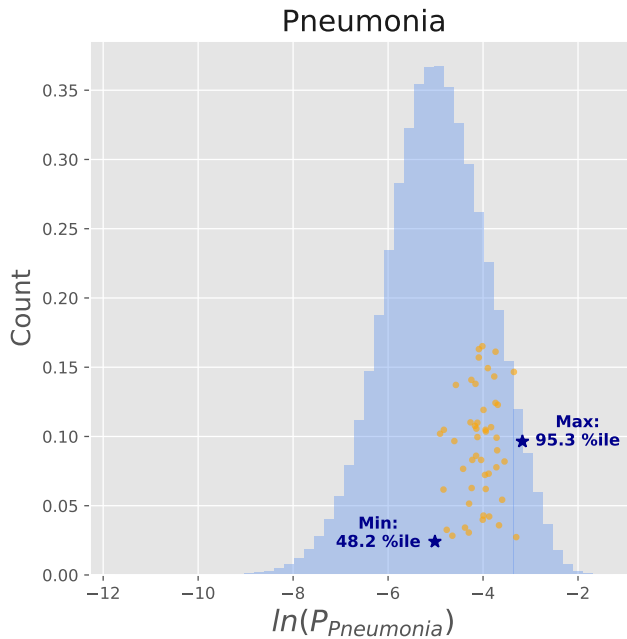


Figure 1: Comparison of the variability in pneumonia prediction made for a single radiograph across trained models (jittered orange dots and blue stars, $n=50$) to the variability of the full test set across trained models (blue histogram, $n=22,433$ cases \times 50 models = 1,121,650). The predicted risk of pneumonia on the single radiograph ranged from the 48.2 to the 95.3 percentile.

The variability in predictions for a given radiograph was substantial across models. An example radiograph classification is shown in Figure 1. Figure 1 compares the variability across models ($n=50$) in predicted probability of pneumonia for this radiograph to the variability of predictions for pneumonia in the full test set ($n=22,433$ cases \times 50 models = 1,121,650 total predictions). In this example, the percentile rank range was $95.3\% - 48.2\% = 47.1\%$. The variability of each finding for this radiograph relative to all predictions for a given finding is shown in Figure 4.

In the full test set ($n=22,433$), the mean coefficient of variation for an individual radiograph over 50 retrainings was 0.543, and mean $\ln(\frac{P_{\max}}{P_{\min}})$ was 2.45 (Table 2, Figure 2); for a model with unvarying predictions, $\ln(\frac{P_{\max}}{P_{\min}})$ would equal zero. The radiographs had a mean percentile rank range of 43.0%. In other words, the average difference between the percentile rank of a radiograph’s highest prediction, relative to all predictions for that finding in the test set, and the radiograph’s lowest prediction of that finding, was 43.0%—nearly half the available range.

Table 2: Average variability metrics for individual models and ensembles. Note that coefficient of variation, σ/μ , is $\text{mean}(\sigma/\mu)$, not $\text{mean}(\sigma)/\text{mean}(\mu)$. Varying the order of the training data resulted in varying predictions for the same radiograph. In the full test set ($n=22,433$), a single radiograph had an average $\ln(P_{\max}/P_{\min})$ of 2.45, coefficient of variation of 0.543, and percentile rank range, $R(P_{\max}) - R(P_{\min})$, of 43.0%. Averaging across ten models significantly reduced this variability.

Finding	Average across individual models (n=50)					Ensemble of 10 runs (n=5)	
	Mean (μ)	Stdev. (σ)	σ/μ	$\ln(\frac{P_{\max}}{P_{\min}})$	%ile rank range	σ	σ/μ
Atelectasis	0.107	0.034	0.449	2.085	0.360	0.011	0.142
Cardiomegaly	0.030	0.014	0.686	2.993	0.404	0.004	0.211
Consolidation	0.041	0.014	0.439	2.046	0.368	0.004	0.133
Edema	0.022	0.009	0.654	2.921	0.378	0.003	0.205
Effusion	0.128	0.033	0.523	2.415	0.309	0.010	0.163
Emphysema	0.023	0.010	0.703	3.033	0.479	0.003	0.219
Nodule	0.056	0.021	0.444	2.029	0.493	0.007	0.140
Pneumonia	0.012	0.004	0.403	1.867	0.451	0.001	0.126
Fibrosis	0.016	0.007	0.531	2.435	0.446	0.002	0.171
Hernia	0.002	0.001	0.608	2.784	0.494	0.0004	0.185
Infiltration	0.172	0.042	0.299	1.401	0.425	0.013	0.091
Mass	0.051	0.022	0.624	2.765	0.493	0.007	0.199
Pleural Thickening	0.029	0.012	0.515	2.367	0.457	0.004	0.162
Pneumothorax	0.046	0.022	0.723	3.196	0.465	0.007	0.227

Averaging model predictions significantly reduced the mean coefficient of variability from 0.543 to 0.169 (t-test 15.96, p-value < 0.0001). The distribution over AUC across models showed a degree of variability in both the full and limited test sets (Figure 3, Table 3). In the limited test set, the empirical variability in predictions did not exceed the average DeLong or bootstrap confidence interval for each model (Table 3). The DeLong and bootstrap 95% confidence intervals for AUC contained the mean AUC across models in 99.7% of cases ($n=698/700$).

Table 3: Mean full test set AUC for each finding, variability across repeated model runs, and comparison with DeLong and bootstrap confidence interval for AUC.

Finding	Full test set (n=22,433)		Limited test set (n=792)			
	Mean AUC	Empirical 95% CI width	Mean AUC	Empirical 95% CI width	Average DeLong 95% CI width	Average bootstrap 95% CI width
Atelectasis	0.817	0.010	0.796	0.029	0.077	0.077
Cardiomegaly	0.906	0.012	0.878	0.037	0.083	0.082
Consolidation	0.802	0.010	0.736	0.030	0.097	0.097
Edema	0.894	0.010	0.879	0.025	0.072	0.071
Effusion	0.883	0.004	0.829	0.018	0.065	0.065
Emphysema	0.923	0.012	0.910	0.028	0.067	0.066
Nodule	0.772	0.011	0.681	0.047	0.111	0.109
Pneumonia	0.760	0.023	0.715	0.054	0.137	0.136
Fibrosis	0.827	0.017	0.836	0.033	0.100	0.100
Hernia	0.911	0.067	0.897	0.082	0.108	0.105
Infiltration	0.712	0.009	0.650	0.030	0.087	0.087
Mass	0.837	0.015	0.766	0.040	0.103	0.103
Pleural Thickening	0.784	0.016	0.725	0.051	0.112	0.111
Pneumothorax	0.873	0.012	0.860	0.031	0.077	0.077

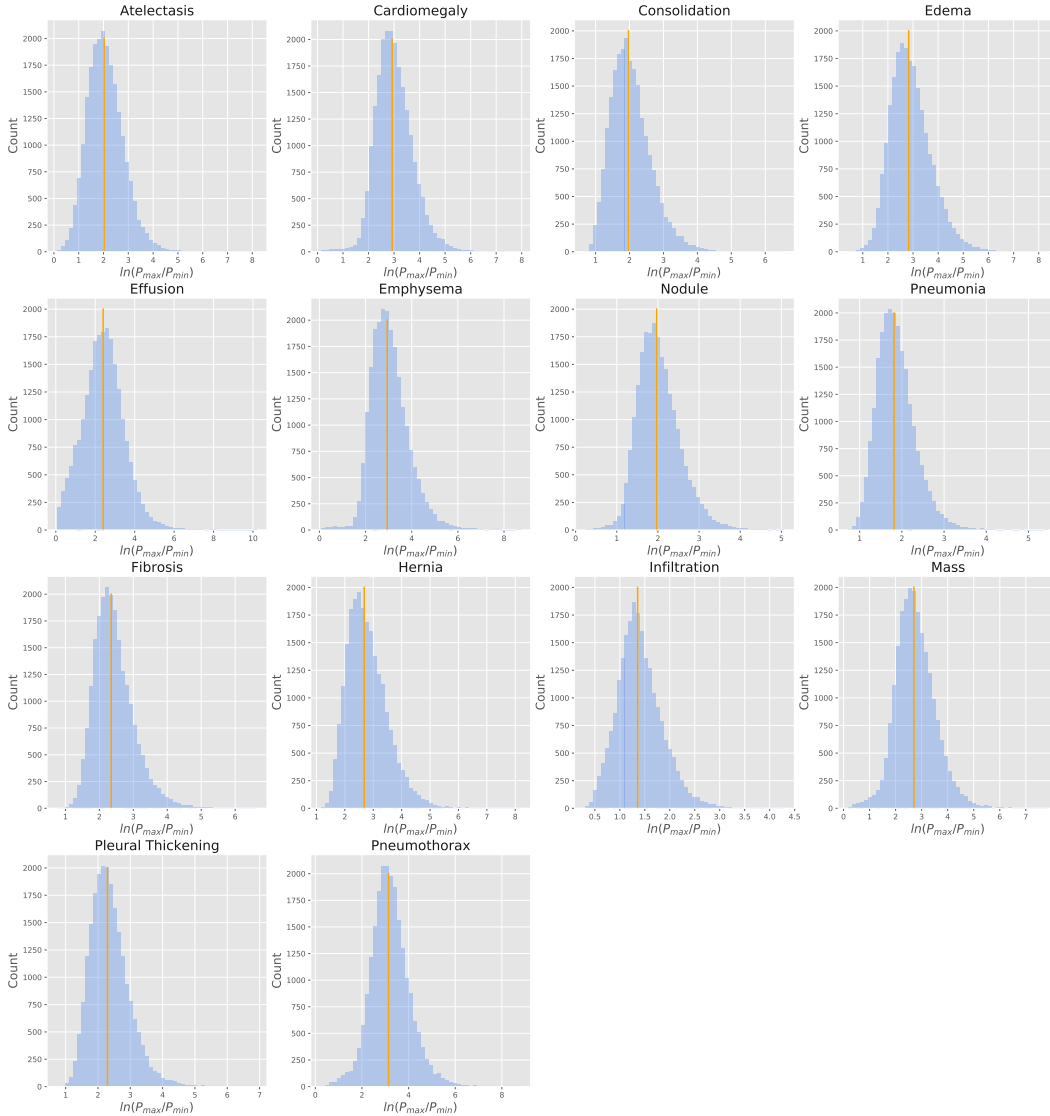


Figure 2: Distribution of $\ln\left(\frac{P_{\max}}{P_{\min}}\right)$ for each finding in the full test set ($n=22,433$), where P_{\max} is the highest and P_{\min} the lowest probability predicted for a given finding on a given radiograph across all 50 models. The mean $\ln\left(\frac{P_{\max}}{P_{\min}}\right)$ was 2.45, indicating substantial variability in predictions made for the same radiograph; models with consistent predictions would have mean $\ln\left(\frac{P_{\max}}{P_{\min}}\right)$ of zero.

4 Discussion

We found substantial variation among the predicted probability of findings when varying the sampling of batches in the training set (mean coefficient of variation across all findings 0.543, mean $\ln(P_{\max}/P_{\min})$ of 2.45; Figure 2, Table 2). We highlighted a case that demonstrated how predicted probabilities could vary across models (Figure 4), shifting its estimated risk relative to the test set population based on the random seed used to train the model. The average case had a 43.0% percentile range between its highest and lowest estimated probability of disease across all 50 models.

We found that there was variability across models in AUC for all findings. The overall AUC for each finding in the full test set of over 20,000 cases was much more stable than the substantial variability in predictions for individual radiographs. As explained by DeLong et al. [46], “the area under the population ROC curve represents the probability that, when the variable is observed for a randomly selected individual from the abnormal population and a randomly selected individual from the normal

population, the resulting values will be in the correct order (e.g., abnormal value higher than the normal value).” In our case, AUC represents the probability that a randomly selected radiograph that is ground-truth positive for pathology will be assigned a higher score by the CNN than a randomly selected radiograph that is ground-truth negative for pathology. Calculating AUC is thus identical to estimating p for a Bernoulli random variable (i.e., a weighted coin-flip) by repeatedly sampling from this distribution and calculating the average \hat{p} over all draws. As our sample size grows larger and larger, our uncertainty interval over the true value of p (and, equivalently, our uncertainty over AUC) grows progressively narrower. AUC can thus be relatively consistent across CNNs that make variable radiograph-level predictions, provided that these variable predictions are similar overall in their ability to classify positive and negative cases.

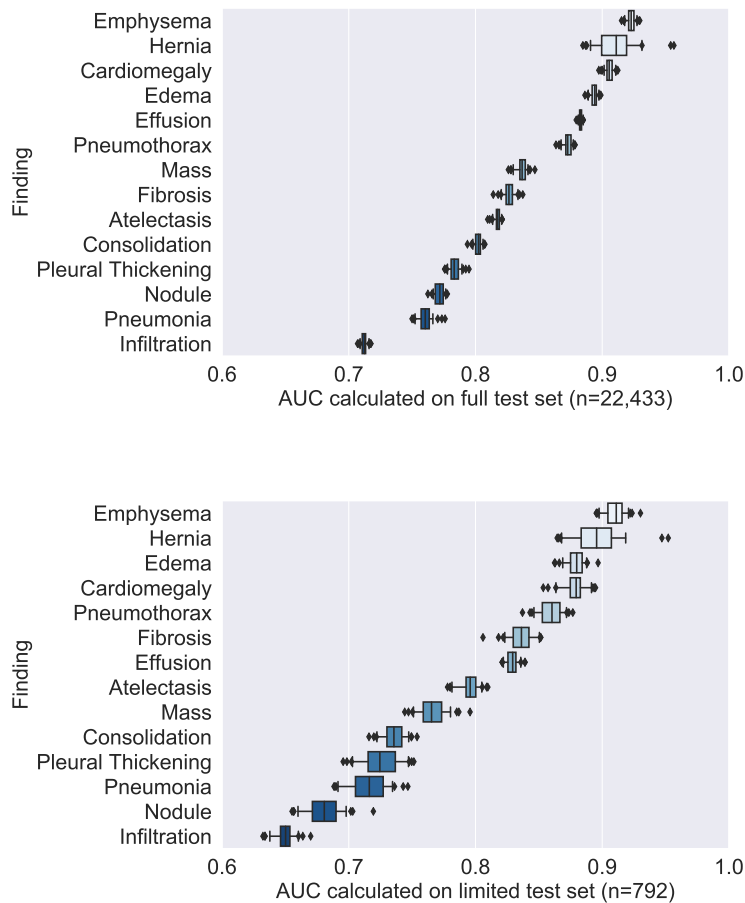


Figure 3: Boxplots of AUC across all 50 models in the full test set ($n=22,433$; top panel) and limited test set, representative of test sets used for expert labeling ($n=792$; bottom panel). Despite substantial individual radiograph-level variability, variability in AUC was low for most findings on the full test set due to the large sample size. The limited test set had expectedly wider distributions over AUC.

The variability in AUC was expectedly wider in the limited test set compared to the full test set. We compared realized variability across models to 95% confidence intervals estimated by two commonly used methods, DeLong and bootstrapping, on the limited test set and found that the realized variability did not exceed these estimated bounds. We note that this comparison is limited and not fully powered; we use sample mean instead of unknown population mean, limiting our ability to detect true differences. Nevertheless, it provides evidence that variability in AUC does not grossly exceed the estimates of common statistical tests, and that these tests can be used to compare the performance of different CNNs, provided researchers are aware of their variability.

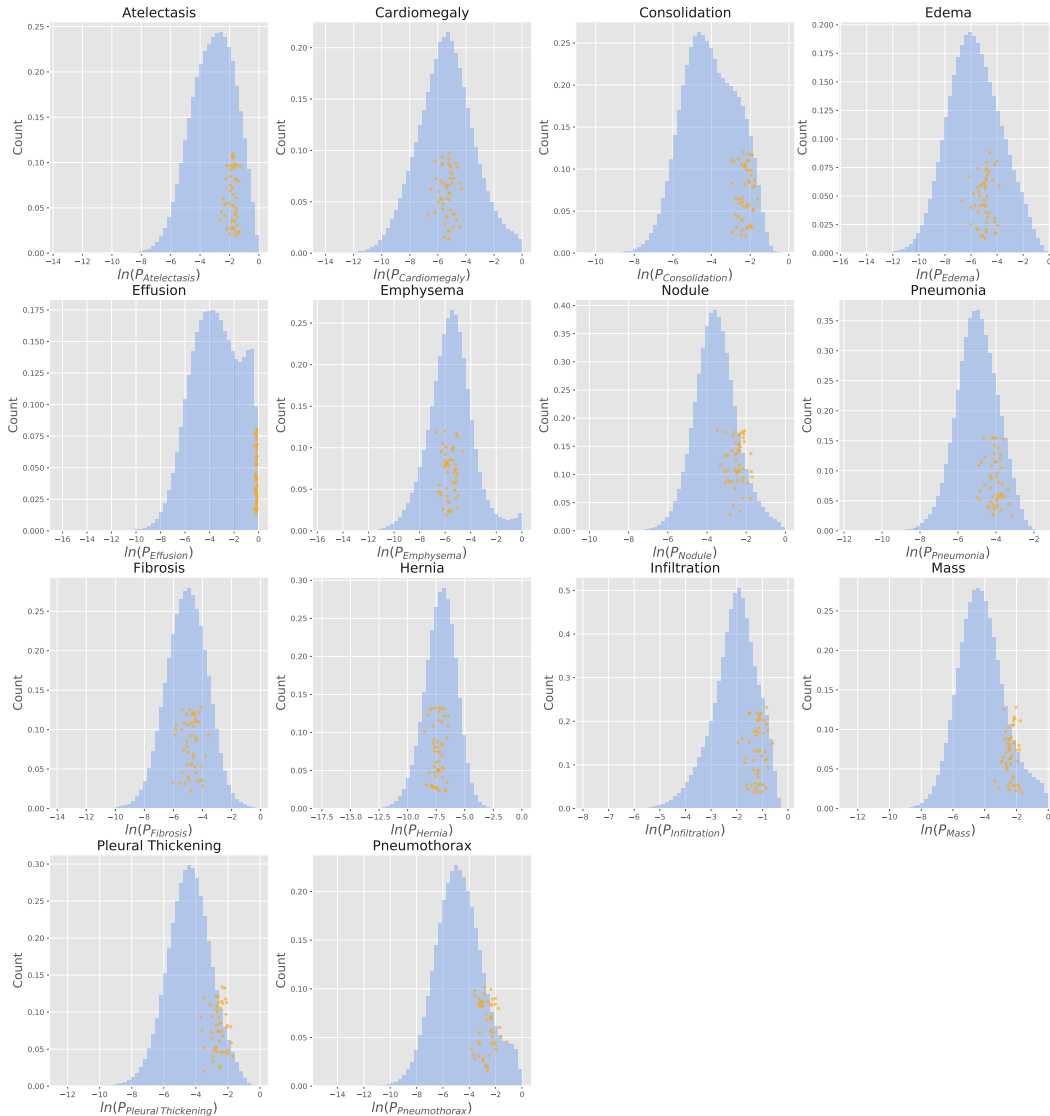


Figure 4: Comparison of the variability in predictions for an example radiograph across models (orange dots; $n=50$ per finding) to distribution of predictions in the full test set (blue histogram; $n=22,433$ cases \times 50 retrainsings = 1,121,650 predictions per finding). For many findings, the estimated risk varied substantially (e.g., Pneumonia).

Stability in AUC across trained models can mask the wide variation in predictions for a single radiograph, and should not reassure researchers that predictions will remain consistent. In our experiments, each DenseNet-121 [39] model was initialized with the same pre-trained weights from ImageNet [40] and trained with the same train/tune/test data, optimizer, and hyperparameters. From this consistent configuration, we fine-tuned each model on the NIH chest radiograph dataset [4], varying only the order in which training data was batched and presented to the model. The substantial variability we observed in predictions for individual radiographs might have been even wider had we allowed the model’s initialization parameters, choice of optimizer, or hyperparameters to vary. [20, 21]. Raghu et al. [47] suggested that pre-training may not be necessary to achieve competitive performance on medical imaging tasks. Our results call to question whether the absence of pre-training may induce additional variability in predictions.

In the context of healthcare, it is particularly important to remain aware of the variability in individual predictions. If deep learning-based decision support will be deployed in clinical settings, their predictions will alter the diagnoses and treatments given to some patients. Justice, beneficence, and

respect for persons are the three ethical principles proposed by the Belmont Report [48], which guides discussion of ethical considerations in medical research. An algorithm that treats identical patients differently challenges the value of justice and potentially leaves the care of patients up to a multi-dimensional coin flip. At the same time, radiologists are also far from perfectly consistent [49]. Rajpurkar et al. [1] observed relatively low inter-rater agreement between the radiologists who contributed the expert labels for pneumonia (0.387 average F1 score comparing each individual radiologist to the majority vote of three other radiologists). Similarly, a study of radiologists at Massachusetts General Hospital found 30% disagreement between colleagues' interpretations of abdominopelvic CTs and 25% disagreement for the same radiologist viewing the CT at different times [50, 49]. Machine learning algorithms may offer an opportunity to improve the consistency of medical decisions, but only if we are attentive to the inconsistency of which they, too, are capable.

Straightforward workarounds, such as averaging predictions across models [24, 31], can substantially mitigate the effect of this individual-level variability (coefficient of variation reduced from 0.543 to 0.169, p -value < 0.0001). Reducing the variability in individual predictions is also likely to improve performance metrics such as AUC; ensembling of CNN predictions has been successfully demonstrated in medical imaging literature [25–29, 2, 30], primarily to optimize model performance. No prior work to our knowledge examines how variability in the predictions of CNNs for radiologic imaging may translate to the care of individual patients. We encourage researchers to be vigilant of the variability of deep learning models and to provide some measure of how consistently their final (possibly ensembled) model performs in predicting findings for individual patients to assure readers that end users of the model will not be fooled by randomness.

Acknowledgments

We would like to thank the Internal Medicine residency program at California Pacific Medical Center (San Francisco, CA) for giving one of the authors (J.Z.) dedicated time to work on this research while he was a preliminary medicine resident.

References

- [1] Pranav Rajpurkar, Jeremy Irvin, Kaylie Zhu, Brandon Yang, Hershel Mehta, Tony Duan, Daisy Ding, Aarti Bagul, Curtis Langlotz, Katie Shpanskaya, Matthew P Lungren, and Andrew Y Ng. CheXNet: radiologist-level pneumonia detection on chest x-rays with deep learning. *arXiv*, November 2017.
- [2] Jeremy Irvin, Pranav Rajpurkar, Michael Ko, Yifan Yu, Silvana Ciurea-Ilcus, Chris Chute, Henrik Marklund, Behzad Haghighi, Robyn Ball, Katie Shpanskaya, Jayne Seekins, David A Mong, Safwan S Halabi, Jesse K Sandberg, Ricky Jones, David B Larson, Curtis P Langlotz, Bhavik N Patel, Matthew P Lungren, and Andrew Y Ng. CheXpert: A large chest radiograph dataset with uncertainty labels and expert comparison. *arXiv*, January 2019.
- [3] Alistair E W Johnson, Tom J Pollard, Seth J Berkowitz, Nathaniel R Greenbaum, Matthew P Lungren, Chih-Ying Deng, Roger G Mark, and Steven Horng. MIMIC-CXR: A large publicly available database of labeled chest radiographs. *arXiv*, January 2019.
- [4] Xiaosong Wang, Yifan Peng, Le Lu, Zhiyong Lu, Mohammadhadi Bagheri, and Ronald M Summers. ChestX-ray8: Hospital-scale chest x-ray database and benchmarks on weakly-supervised classification and localization of common thorax diseases. *arXiv*, May 2017.
- [5] Xiaosong Wang, Yifan Peng, Le Lu, Zhiyong Lu, and Ronald M Summers. TieNet: Text-image embedding network for common thorax disease classification and reporting in chest x-rays. *arXiv*, January 2018.
- [6] John R Zech, Marcus A Badgeley, Manway Liu, Anthony B Costa, Joseph J Titano, and Eric Karl Oermann. Variable generalization performance of a deep learning model to detect pneumonia in chest radiographs: A cross-sectional study. *PLoS Med.*, 15(11):e1002683, November 2018.
- [7] D Sculley, Gary Holt, Daniel Golovin, Eugene Davydov, Todd Phillips, Dietmar Ebner, Vinay Chaudhary, Michael Young, Jean-Francois Crespo, and Dan Dennison. Hidden technical debt in machine learning systems. In *Proceedings of the 28th International Conference on Neural*

- Information Processing Systems - Volume 2*, NIPS'15, pages 2503–2511, Cambridge, MA, USA, 2015. MIT Press.
- [8] N Papernot, P McDaniel, S Jha, and others. The limitations of deep learning in adversarial settings. *2016 IEEE European*, 2016.
 - [9] Ali Rahimi. Let's take machine learning from alchemy to electricity (test-of-time award presentation). *NeurIPS*, 2017.
 - [10] Samuel G Finlayson, John D Bowers, Joichi Ito, Jonathan L Zittrain, Andrew L Beam, and Isaac S Kohane. Adversarial attacks on medical machine learning. *Science*, 363(6433):1287–1289, March 2019.
 - [11] Jessica Zosa Forde and Michela Paganini. The scientific method in the science of machine learning. *arXiv*, April 2019.
 - [12] Ashish Vaswani, Noam Shazeer, Niki Parmar, Jakob Uszkoreit, Llion Jones, Aidan N Gomez, Ł Ukasz Kaiser, and Illia Polosukhin. Attention is all you need. In I Guyon, U V Luxburg, S Bengio, H Wallach, R Fergus, S Vishwanathan, and R Garnett, editors, *Advances in Neural Information Processing Systems 30*, pages 5998–6008. Curran Associates, Inc., 2017.
 - [13] Gábor Melis, Chris Dyer, and Phil Blunsom. On the state of the art of evaluation in neural language models. In *ICLR*, 2018.
 - [14] Mario Lucic, Karol Kurach, Marcin Michalski, Sylvain Gelly, and Olivier Bousquet. Are GANs created equal? a Large-Scale study. In *NeurIPS*, 2018.
 - [15] Carlos Riquelme, George Tucker, and Jasper Snoek. Deep Bayesian bandits showdown: An empirical comparison of Bayesian deep networks for Thompson sampling. In *ICLR 2018*, February 2018.
 - [16] Peter Henderson, Riashat Islam, Philip Bachman, Joelle Pineau, Doina Precup, and David Meger. Deep reinforcement learning that matters. In *Thirty-Second AAAI Conference on Artificial Intelligence*, April 2018.
 - [17] William Gale, Luke Oakden-Rayner, Gustavo Carneiro, Andrew P Bradley, and Lyle J Palmer. Detecting hip fractures with radiologist-level performance using deep neural networks. *arXiv*, November 2017.
 - [18] Simukayi Mutasa, Peter D Chang, Carrie Ruzal-Shapiro, and Rama Ayyala. MABAL: a novel deep-learning architecture for machine-assisted bone age labeling. *J. Digit. Imaging*, 31(4): 513–519, August 2018.
 - [19] Xiaosong Wang, Yifan Peng, Le Lu, Zhiyong Lu, and Ronald M Summers. Tienet: Text-image embedding network for common thorax disease classification and reporting in chest x-rays. In *Proceedings of the IEEE conference on computer vision and pattern recognition*, pages 9049–9058, 2018.
 - [20] Ashia C Wilson, Rebecca Roelofs, Mitchell Stern, Nati Srebro, and Benjamin Recht. The marginal value of adaptive gradient methods in machine learning. In I Guyon, U V Luxburg, S Bengio, H Wallach, R Fergus, S Vishwanathan, and R Garnett, editors, *Advances in Neural Information Processing Systems 30*, pages 4148–4158. Curran Associates, Inc., 2017.
 - [21] Dami Choi, Christopher J Shallue, Zachary Nado, Jaehoon Lee, Chris J Maddison, and George E Dahl. On empirical comparisons of optimizers for deep learning. October 2019.
 - [22] Andre Esteva, Brett Kuprel, Roberto A Novoa, Justin Ko, Susan M Swetter, Helen M Blau, and Sebastian Thrun. Dermatologist-level classification of skin cancer with deep neural networks. *Nature*, 542(7639):115–118, February 2017.
 - [23] P D Chang, E Kuoy, J Grinband, B D Weinberg, M Thompson, R Homo, J Chen, H Abcede, M Shafie, L Sugrue, C G Filippi, M-Y Su, W Yu, C Hess, and D Chow. Hybrid 3D/2D convolutional neural network for hemorrhage evaluation on head CT. *AJNR Am. J. Neuroradiol.*, 39(9):1609–1616, September 2018.

- [24] Peter Sollich and Anders Krogh. Learning with ensembles: How overfitting can be useful. In D S Touretzky, M C Mozer, and M E Hasselmo, editors, *Advances in Neural Information Processing Systems 8*, pages 190–196. MIT Press, 1996.
- [25] Joseph J Titano, Marcus Badgeley, Javin Schefflein, Margaret Pain, Andres Su, Michael Cai, Nathaniel Swinburne, John Zech, Jun Kim, Joshua Bederson, J Mocco, Burton Drayer, Joseph Lehar, Samuel Cho, Anthony Costa, and Eric K Oermann. Automated deep-neural-network surveillance of cranial images for acute neurologic events. *Nat. Med.*, 24(9):1337–1341, September 2018.
- [26] Nan Wu, Jason Phang, Jungkyu Park, Yiqiu Shen, Zhe Huang, Masha Zorin, Stanisław Jastrzębski, Thibault Févry, Joe Katsnelson, Eric Kim, Stacey Wolfson, Ujas Parikh, Sushma Gaddam, Leng Leng Young Lin, Kara Ho, Joshua D Weinstein, Beatriu Reig, Yiming Gao, Hildegard Toth, Kristine Pysarenko, Alana Lewin, Jiyon Lee, Krystal Airola, Eralda Mema, Stephanie Chung, Esther Hwang, Naziya Samreen, S Gene Kim, Laura Heacock, Linda Moy, Kyunghyun Cho, and Krzysztof J Geras. Deep neural networks improve radiologists’ performance in breast cancer screening. *arXiv*, March 2019.
- [27] Pranav Rajpurkar, Jeremy Irvin, Aarti Bagul, Daisy Ding, Tony Duan, Hershel Mehta, Brandon Yang, Kaylie Zhu, Dillon Laird, Robyn L Ball, Curtis Langlotz, Katie Shpanskaya, Matthew P Lungren, and Andrew Ng. MURA dataset: Towards radiologist-level abnormality detection in musculoskeletal radiographs. *arXiv*, December 2017.
- [28] Varun Gulshan, Lily Peng, Marc Coram, Martin C Stumpe, Derek Wu, Arunachalam Narayanaswamy, Subhashini Venugopalan, Kasumi Widner, Tom Madams, Jorge Cuadros, Ramasamy Kim, Rajiv Raman, Philip C Nelson, Jessica L Mega, and Dale R Webster. Development and validation of a deep learning algorithm for detection of diabetic retinopathy in retinal fundus photographs. *JAMA*, 316(22):2402–2410, December 2016.
- [29] Pranav Rajpurkar, Jeremy Irvin, Robyn L Ball, Kaylie Zhu, Brandon Yang, Hershel Mehta, Tony Duan, Daisy Ding, Aarti Bagul, Curtis P Langlotz, Bhavik N Patel, Kristen W Yeom, Katie Shpanskaya, Francis G Blankenberg, Jayne Seekins, Timothy J Amrhein, David A Mong, Safwan S Halabi, Evan J Zucker, Andrew Y Ng, and Matthew P Lungren. Deep learning for chest radiograph diagnosis: A retrospective comparison of the CheXNeXt algorithm to practicing radiologists. *PLoS Med.*, 15(11):e1002686, November 2018.
- [30] Ian Pan, Hans Henrik Thodberg, Safwan S Halabi, Jayashree Kalpathy-Cramer, and David B Larson. Improving automated pediatric bone age estimation using ensembles of models from the 2017 RSNA machine learning challenge. *Radiology: Artificial Intelligence*, 1(6):e190053, November 2019.
- [31] Balaji Lakshminarayanan, Alexander Pritzel, and Charles Blundell. Simple and scalable predictive uncertainty estimation using deep ensembles. In I Guyon, U V Luxburg, S Bengio, H Wallach, R Fergus, S Vishwanathan, and R Garnett, editors, *Advances in Neural Information Processing Systems 30*, pages 6402–6413. Curran Associates, Inc., 2017.
- [32] Yaniv Ovadia, Emily Fertig, Jie Ren, Zachary Nado, D Sculley, Sebastian Nowozin, Joshua V Dillon, Balaji Lakshminarayanan, and Jasper Snoek. Can you trust your model’s uncertainty? evaluating predictive uncertainty under dataset shift. June 2019.
- [33] Luis Carlos Silva-Ayçaguer, Patricio Suárez-Gil, and Ana Fernández-Somoano. The null hypothesis significance test in health sciences research (1995-2006): statistical analysis and interpretation. *BMC Med. Res. Methodol.*, 10:44, May 2010.
- [34] P Schulam and S Saria. Can you trust this prediction? Auditing pointwise reliability after learning. *The 22nd International Conference on*, 2019.
- [35] Maithra Raghu, Katy Blumer, Rory Sayres, Ziad Obermeyer, Bobby Kleinberg, Sendhil Mul-lainathan, and Jon Kleinberg. Direct uncertainty prediction for medical second opinions. In Kamalika Chaudhuri and Ruslan Salakhutdinov, editors, *Proceedings of the 36th International Conference on Machine Learning*, volume 97 of *Proceedings of Machine Learning Research*, pages 5281–5290, Long Beach, California, USA, 2019. PMLR.

- [36] M W Dusenberry, D Tran, E Choi, J Kemp, J Nixon, G Jerfel, K Heller, and A M Dai. Analyzing the role of model uncertainty for electronic health records. *ICML Workshop on Uncertainty & Robustness in Deep Learning*, 2019.
- [37] Meire Fortunato, Charles Blundell, and Oriol Vinyals. Bayesian recurrent neural networks. April 2017.
- [38] John Zech. reproduce-chexnet, 2018. URL <https://github.com/jrzech/reproduce-chexnet>.
- [39] Gao Huang, Zhuang Liu, Laurens Van Der Maaten, and Kilian Q Weinberger. Densely connected convolutional networks. In *Proceedings of the IEEE conference on computer vision and pattern recognition*, pages 4700–4708, 2017.
- [40] Olga Russakovsky, Jia Deng, Hao Su, Jonathan Krause, Sanjeev Satheesh, Sean Ma, Zhiheng Huang, Andrej Karpathy, Aditya Khosla, Michael Bernstein, Alexander C Berg, and Li Fei-Fei. ImageNet large scale visual recognition challenge. *Int. J. Comput. Vis.*, 115(3):211–252, December 2015.
- [41] Xavier Robin, Natacha Turck, Alexandre Hainard, Natalia Tiberti, Frédérique Lisacek, Jean-Charles Sanchez, and Markus Müller. pROC: an open-source package for R and S+ to analyze and compare ROC curves. *BMC Bioinformatics*, 12:77, March 2011.
- [42] Ross Ihaka and Robert Gentleman. R: A language for data analysis and graphics. *J. Comput. Graph. Stat.*, 5(3):299–314, September 1996.
- [43] E R DeLong, D M DeLong, and D L Clarke-Pearson. Comparing the areas under two or more correlated receiver operating characteristic curves: a nonparametric approach. *Biometrics*, 44(3):837–845, September 1988.
- [44] J Carpenter and J Bithell. Bootstrap confidence intervals: when, which, what? a practical guide for medical statisticians. *Stat. Med.*, 19(9):1141–1164, May 2000.
- [45] H B Mann and D R Whitney. On a test of whether one of two random variables is stochastically larger than the other. *Ann. Math. Stat.*, 18(1):50–60, March 1947.
- [46] Elizabeth R. DeLong, David M. DeLong, and Daniel L. Clarke-Pearson. Comparing the areas under two or more correlated receiver operating characteristic curves: A nonparametric approach. *Biometrics*, 44(3):837–845, 1988. ISSN 0006341X, 15410420.
- [47] M Raghu, C Zhang, J Kleinberg, and S Bengio. Transfusion: Understanding transfer learning with applications to medical imaging. *arXiv preprint arXiv*, 2019.
- [48] National Commission for the Protection of Human Subjects of Biomedical and Behavioral Research. *The Belmont Report: Ethical Principles and Guidelines for the Protection of Human Subjects of Research*. The Commission, 1978.
- [49] Michael A Bruno, Eric A Walker, and Hani H Abujudeh. Understanding and confronting our mistakes: The epidemiology of error in radiology and strategies for error reduction. *Radiographics*, 35(6):1668–1676, October 2015.
- [50] Hani H Abujudeh, Giles W Boland, Rathachai Kaewlai, Pavel Rabiner, Elkarn F Halpern, G Scott Gazelle, and James H Thrall. Abdominal and pelvic computed tomography (CT) interpretation: discrepancy rates among experienced radiologists. *Eur. Radiol.*, 20(8):1952–1957, August 2010.